ACS Chemical Neuroscience

Article

N1-Substituted Quinoxaline-2,3-diones as Kainate Receptor Antagonists: X-ray Crystallography, Structure-Affinity Relationships and in vitro Pharmacology

Jakob S. Pallesen, Stine Møllerud, Karla Frydenvang, Darryl S. Pickering, Jan Bornholdt, Birgitte Nielsen, Diletta Pasini, Liwei Han, Laura Marconi, Jette Sandholm Kastrup, and Tommy N. Johansen

ACS Chem. Neurosci., **Just Accepted Manuscript** • DOI: 10.1021/acschemneuro.8b00726 • Publication Date (Web): 08 Jan 2019

*N*1-Substituted Quinoxaline-2,3-diones as Kainate Receptor Antagonists: X-ray Crystallography, Structure-Affinity Relationships and *in vitro* Pharmacology

Jakob Pallesen, Stine Møllerud, Karla Frydenvang, Darryl S. Pickering,* Jan Bornholdt,† Birgitte Nielsen, Diletta Pasini, Liwei Han, Laura Marconi, Jette Sandholm Kastrup and Tommy N. Johansen**

Department of Drug Design and Pharmacology, Faculty of Health and Medical Sciences, University of Copenhagen, DK-2100 Copenhagen, Denmark.

ABSTRACT

Among the ionotropic glutamate receptors, the physiological role of kainate receptors is less well understood. Although ligands with selectivity towards the kainate receptor subtype GluK1 are available, tool compounds with selectivity at the remaining kainate receptor subtypes are sparse. Here, we have synthesized a series of quinoxaline-2,3-diones with substitutions in the *N*1-, 6- and 7-position to investigate the structure-activity relationship (SAR) at GluK1-3 and GluK5. Pharmacological characterization at native and recombinant kainate and AMPA receptors revealed that compound **37** had a GluK3-binding affinity (K_i) of 0.142 μM and 8-fold preference for GluK3 over GluK1. Despite lower binding affinity of **22** at GluK3 (K_i = 2.91 μM) its preference for GluK3 over GluK1 and GluK2 was >30-fold. Compound **37** was crystallized with the GluK1 ligand-binding domain to understand the SAR. The X-ray structure showed that **37** stabilized the protein in an open conformation, consistent with an antagonist binding mode.

Keywords: quinoxalinediones, kainate receptors, antagonists, structure-activity studies, x-ray crystallography, binding affinities

INTRODUCTION

(*S*)-Glutamate (Glu) activates two main classes of central nervous system receptors: metabotropic glutamate receptors (mGluRs) and ionotropic glutamate receptors (iGluRs). The mGluRs are G-protein-coupled receptors that mediate a signaling cascade inside the neurons, whereas the iGluRs are ligand-gated ion channels, which are essential for mediating fast synaptic transmission. The iGluRs consist of three subfamilies, named after their response to the small molecule agonists AMPA, NMDA, and kainate.[1] AMPA and NMDA receptors are well known for their fundamental involvement in several brain disorders, such as epilepsy, pain and neurodegenerative disorders,[1-4] but so far AMPA and NMDA receptors have been shown to be difficult therapeutic targets to handle mainly due to a deep involvement of both NMDA and AMPA receptors in many physiological processes. In contrast to AMPA and NMDA receptors which are localized postsynaptically, kainate receptors are found both pre- and postsynaptically and are believed to have a modulatory function in central nervous system neurotransmission.[1, 5, 6] Compared to AMPA and NMDA receptors, kainate receptors are less well characterized,

mainly due to a lack of selective agonists and antagonists, and this fact has impeded the understanding of the physiological and pharmacological potential of kainate receptors as drug targets. Some of the first antagonists to be used in kainate receptor research were the 1,4-dihydroquinoxaline-2,3-diones (QXs), such as CNQX, as well as the isoxazole-based acidic amino acid (*S*)-ATPO (Figure 1).[7] Today, only one structure of the ligand-binding domain (LBD) of GluK1 has been determined in complex with a quinoxalinedione (compound **2**),[8] containing one substituent different from hydrogen in the 6-position. So far, it has not been possible to crystallize the LBDs of GluK2-5 with antagonists.

However, neither of the early compounds are optimal for kainate receptor research as they are better antagonists of AMPA receptors than of kainate receptors. Later on, GluK1 receptor-preferring amino acid-based antagonists have been reported, such as the substituted willardiine UBP310 and the substituted tetrahydroisoquinoline LY 466195. Using such GluK1 receptor-preferring antagonists, kainate receptors and especially GluK1-containing kainate receptors have been demonstrated to be putative targets in disorders such as epilepsy, pain and migraine.[5, 7] However, due to lack of selective antagonists for the remaining kainate receptors, the physiological role and therapeutic

potential of these receptors are still unclear. Only a few GluK2- and/or GluK3-preferring compounds have been reported. One interesting example is the GluK3-preferring *N*1-substituted quinoxaline-2,3-dione LU 97175 (compound **1**) reported to have a sub-micromolar affinity at GluK3 receptors as well as a 4-fold and >10-fold preference for GluK3 over GluK1 and GluK2 receptors, respectively.[9] Furthermore, compound **1** was able to block AMPA-induced cell death *in vitro* and had anticonvulsant activities in rat kindling studies.[9] More recently, another series of new quinoxaline-2,3-diones represented by compounds **2** and **3** has been reported (Figure 1).[8, 10] Whereas compound **2** showed mid-micromolar affinity with no selectivity among the recombinant receptors tested (GluA2, GluK1–3), compound **3** showed a preference for GluK3 over GluK1,2 and in particular over GluA2-receptors.

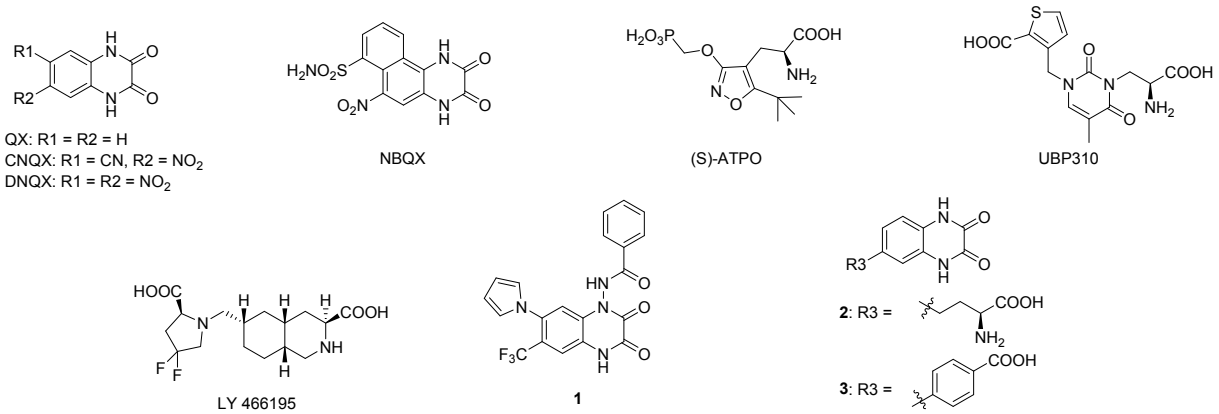

Figure 1. Chemical structures of selected AMPA/kainate receptor antagonists.

In the effort to identify tools useful for the pharmacological characterization of native kainate receptors, we prepared a series of quinoxaline-2,3-diones substituted in the 1-position, 6-position and 7-position, and characterized the compounds in radioligand receptor binding assays using native and recombinant receptors. Besides at GluA2 and GluK1-3, the new compounds were characterized with respect to binding affinity at the kainate receptor GluK5 at which only a limited number of compounds have been tested.[11] Furthermore, compound **1** was studied in a two-electrode voltage clamp (TEVC) assay using recombinant GluK1, GluK2 and GluK3 receptors expressed in *Xenopus laevis* oocytes. Finally, in order to understand the molecular interaction of this series of compounds with kainate receptors, we report an X-ray structure of one of the new

compounds, compound **37**, co-crystallized together with the GluK1 ligand-binding domain (LBD). Notably, four of the new compounds (**19**, **21**, **22** and **37**) showed preference for the GluK3 receptor, for which a need of potent and selective ligands exists.

RESULTS AND DISCUSSION

Chemistry. Compound (**1**, LU 97175) was synthesized as shown in Scheme 1 according to the procedures described by Lubisch *et al.*[12] The chlorine of **4** could easily be substituted by benzhydrazide to give **5** which underwent acylation, reduction and ring closure to form compound **6**. Dinitration of **6** to **7** was followed by hydrolysis of the benzamide bond to give **8**. Compound **8** was acylated with various acylating agents to give target compounds **9** – **12**. Finally, the nitro group of compound **12** was reduced to the corresponding amine, which was directly converted into the corresponding pyrrole **1**.

Scheme 1. Synthesis of target compounds 1 and 6 – 12.[a]

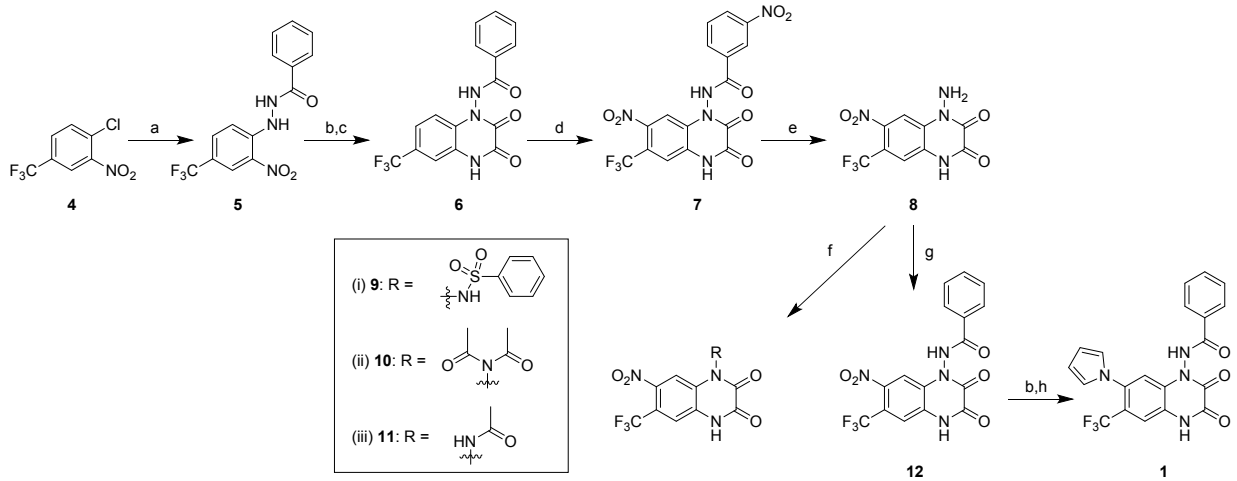

[a] Reagents and conditions: (a) benzhydrazide, K_2CO_3, DMF, 110 °C, 4 h; (b) ethyl chlorooxoacetate, TEA, dry THF; (c) iron powder, AcOH, reflux, 30 min; (d) KNO_3, H_2SO_4, 0 °C, 1 h; (e) 90% H_2SO_4, 80 °C, 12 h; (f) (i) benzenesulfonyl chloride, *N*-methylimidazole, dry DMSO, rt, 10 min; (ii) Ac_2O, reflux, 1 h; (iii) AcCl, *N*-methylimidazole, dry DMSO, rt,

several days; (g) benzoyl chloride, *N*-methylimidazole, dry DMSO, rt, 10 min; (h) 2,5-dimethoxytetrahydrofurane, AcOH, reflux, 10 min.

The aryl bromide **13** and the aryl iodide **16** were used as starting material for the synthesis of the 7-bromo and the 7-iodo analogues (**15** and **18**, respectively) (Scheme 2). In both cases the fluorides were selectively substituted by benzhydrazide to give **14** and **17**, respectively, which underwent acylation, reduction and ring closure to compounds **15** and **18**, respectively. Compound **18** was also used as starting material in Sonogashira cross coupling reactions to give the 7-alkynes **19** – **22**. The two target quinoxaline-2,3-diones (**24** and **27**) were successfully synthesized starting out from arylhalides **4** and commercial available 1-fluoro-2-nitro-4-(trifluoromethyl)benzene (**25**), respectively, following a procedure similar to that of the synthesis of target compound **15** from arylhalide **13**.

Scheme 2. Synthesis of target compounds 15, 18 – 22, 24 and 27.[a]

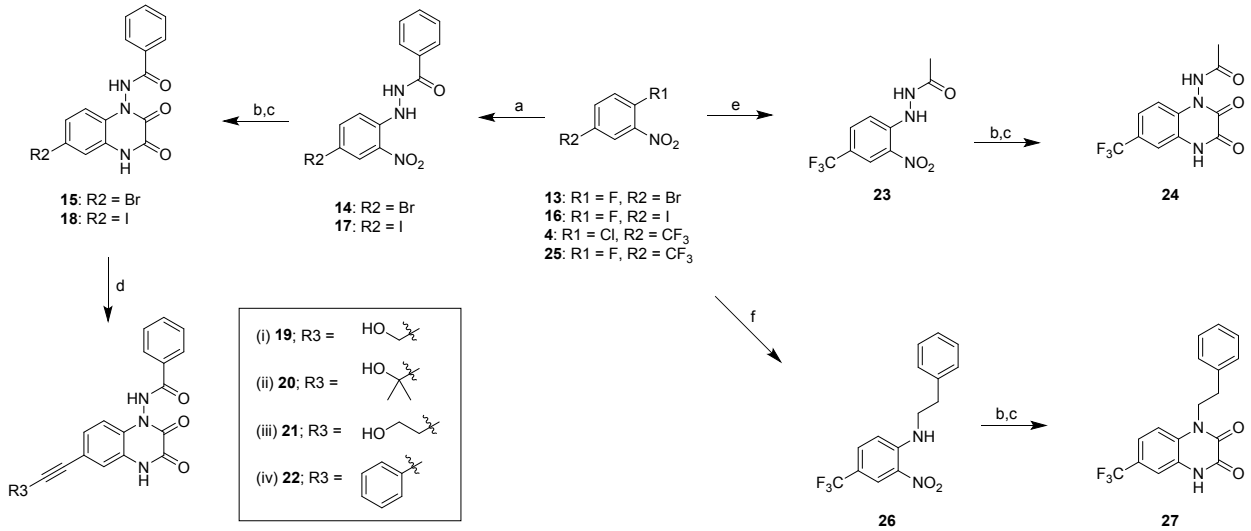

[a] Reagents and conditions: (a) benzhydrazide, DMA, microwave, 160 °C, 30 min; (b) ethyl chlorooxoacetate, TEA, dry THF; (c) iron powder, AcOH, reflux; (d) DMF, Et_2NH, $Pd(dppf)Cl_2{\cdot}DCM$, CuI, (i) propargyl alcohol, (ii) 2-methyl-3-butyn-2-ol, (iii) 3-butynol, (iv) phenylacetylene; (e) acetohydrazide, DMF, 120 °C, 2 h; (f) 2-phenylethan-1-amine, DIPEA, MeCN, rt, 2 h.

Target compounds **33** – **39** were synthesized via the *N*1-amino substituted key intermediate and target compound **32** as shown in Scheme 3. Commercially available **28** was selectively nitrated to give **29**, which was converted to the corresponding difluorosubstituted compound, **30**, to increase the reactivity in the following substitution reaction. Using Boc-protected hydrazine it was possible to selectively substitute one of

the two fluoro substituents to give compound **31**. Attempts to acylate the aromatic nitrogen of compound **31** and then to reduce the nitro group using iron in acetic acid failed. However, the key quinoxalinedione **32** was prepared using a one-pot procedure, first reducing the nitro group of **31** with hydrogen and Pd/C and then converting the amino intermediate into compound **32** using oxalyl chloride.

Scheme 3. Synthesis of target compounds 32 – 39.[a]

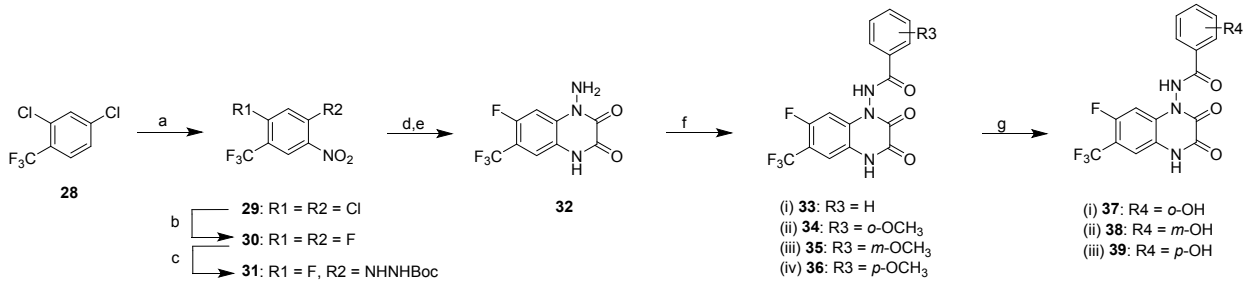

[a] Reagents and conditions: (a) KNO_3, conc. H_2SO_4, rt, 18 h; (b) KF, DMF, 160 °C, 2.5 h; (c) *tert*-butyl hydrazinecarboxylate, dry DMSO, rt, 30 min; (d) 5% Pd/C, H_2 (60 psi), EtOH, rt, 17 h; (e) oxalyl chloride, 1,2-dichlorobenzene 90 °C, 1h; (f) (i) benzoyl chloride, chlorobenzene, 135 °C, 24 h; (ii) 2-methoxybenzoyl chloride, chlorobenzene, 135 °C, 3 days; (iii) 3-methoxybenzoyl chloride, chlorobenzene, 135 °C, 24 h; (iv) 4-methoxybenzoyl chloride, chlorobenzene, 135 °C, 3 days; (g) (i) piperazine, dimethyl acetamide, 150 °C, 8 h; (ii) and (iii) boron tribromide, dry DCM, rt, 48 h.

In order to selectively acylate the exocyclic nitrogen atom in compound **32**, acylation was tried under basic condition using TEA. However, this approach resulted exclusively

in acylation at the *N*4-position of the quinoxalinedione. By performing the acylation without base, but at higher temperature, selective exocyclic acylation was achieved, even though long reaction times were needed. As illustrated in Scheme 3, compound **32** was successfully acylated to **33** – **36** using the appropriate acyl chlorides in refluxing chlorobenzene. Cleavage of the methyl ethers **34** – **36** was initially attempted using boron tribromide in DCM.[13] The method was feasible only for the synthesis of compound **38** and **39**. In case of the ortho-substituted compound **37**, the final demethylation was successfully carried out under basic conditions using piperazine in dimethyl acetamide at 150 °C.[14]

Pharmacology. The *N*1-substituted quinoxaline-2,3-diones and the reference compounds investigated in the present study were characterized in receptor binding studies at native and recombinant iGluRs. Binding affinities are summarized in Table 1.

Table 1. Receptor binding affinities (mean ± SEM) at native and recombinant rat iGluRs.

Com-pound	Native rat iGluR	Recombinant homomeric rat iGluR				
	K_i (μM)	K_i (μM)				
	AMPA	GluK1	GluK2	GluK3	GluK5	GluA2
QX	n.d.[a]	422 ± 146	187 ± 14	129 ± 10	> 1,000	467 ± 82
CNQX	n.d.	1.28 ± 0.30[b]	1.49 ± 0.10[b]	0.637 ± 0.050[b]	8.40 ± 0.88[c]	0.333 ± 0.028[b]
DNQX	n.d.	0.652 ± 0.028[b]	2.10 ± 0.32[b]	0.362 ± 0.033[b]	7.12 ± 0.91	0.254 ± 0.014[b]
NBQX	n.d.	2.60 ± 0.14	5.38 ± 1.24	3.36 ± 0.61	152 ± 23	0.0773 ± 0.0102
1	0.51 ± 0.07	0.697 ± 0.123	0.488 ± 0.058	0.187 ± 0.021	23.9 ± 4.0	1.52 ± 0.25
6	2.24 ± 0.43	1.53 ± 0.17	2.64 ± 0.81	0.726 ± 0.077	103 ± 32	8.34 ± 0.64
7	1.90 ± 0.39	1.42 ± 0.14	2.33 ± 0.34	0.458 ± 0.085	107 ± 39	3.51 ± 0.68
8	2.74 ± 0.30	19.0 ± 2.1	27.4 ± 3.5	14.0 ± 2.6	> 100	11.2 ± 2.4
9	0.53 ± 0.06	1.40 ± 0.42	1.51 ± 0.13	0.916 ± 0.135	78 ± 16	1.55 ± 0.30
10	n.d.	36.8 ± 4.7	20.3 ± 2.7	5.97 ± 0.56	> 100	44.6 ± 11.1
11	n.d.	11.3 ± 0.30	22.6 ± 3.6	7.06 ± 0.64	> 100	27.4 ± 2.7
12	1.91 ± 0.29	1.08 ± 0.11	2.02 ± 0.09	0.526 ± 0.150	43.4 ± 10.9	4.93 ± 0.59
15	1.63 ± 0.25	2.54 ± 0.67	3.33 ± 0.20	0.983 ± 0.059	77 ± 5	8.93 ± 1.18
18	1.36 ± 0.06	1.31 ± 0.30	1.96 ± 0.32	0.379 ± 0.020	42.3 ± 7.9	7.83 ± 0.99
19	n.d.	15.9 ± 1.7	9.78 ± 0.45	1.19 ± 0.10	≈ 100	37.4 ± 4.6
20	n.d.	> 100	> 100	≈ 100	> 100	> 100

21	n.d.	12.7 ± 0.8	n.d	1.10 ± 0.14	n.d.	> 100
22	n.d.	> 100	≈ 100	2.91 ± 0.29	> 100	23.6 ± 6.0
24	n.d.	17.4 ± 1.2	22.4 ± 2.0	8.83 ± 0.78	> 100	32.4 ± 5.0
27	n.d.	10.7 ± 0.7	11.1 ± 2.3	5.86 ± 0.20	> 100	15.3 ± 4.2
32	4.17 ± 0.30	12.6 ± 1.8	14.0 ± 1.3	5.24 ± 0.55	> 100	22.7 ± 7.3
33	n.d.	0.802 ± 0.111	0.813 ± 0.084	0.277 ± 0.031	30.9 ± 3.7	6.15 ± 1.40
34	1.41 ± 0.17	4.35 ± 0.92	1.20 ± 0.25	1.35 ± 0.19	> 100	8.96 ± 1.42
35	0.95 ± 0.12	1.76 ± 0.45	1.85 ± 0.57	0.487 ± 0.078	46.8 ± 5.3	4.56 ± 0.76
36	2.91 ± 0.44	4.74 ± 0.33	2.93 ± 0.25	0.970 ± 0.177	≈ 100	9.87 ± 1.26
37	0.96 ± 0.02	1.12 ± 0.14	0.908 ± 0.167	0.142 ± 0.015	26.4 ± 2.2	4.12 ± 0.61
38	0.72 ± 0.05	0.80 ± 0.18	0.842 ± 0.185	0.329 ± 0.010	45.2 ± 3.6	6.02 ± 0.10
39	2.07 ± 0.43	2.15 ± 0.36	2.94 ± 0.09	1.79 ± 0.56	> 100	5.90 ± 0.40

[a] n.d.: not determined. [b] Ref. 9. [c] Ref 14.

Whereas the *N*1-unsubstituted reference quinoxaline-2,3-diones QX, CNQX and DNQX showed no appreciable preference among the AMPA and the kainate receptors GluK1-3, NBQX had a marked preference for GluA2 receptors as compared to kainate receptors GluK1-3 (34-70-fold preference). The *N*1-substituted reference quinoxaline-2,3-dione

(compound **1**, LU 97175) showed 2-8-fold preference for GluK1-3 over GluA2. Among the recombinant kainate receptors, compound **1** showed a 4-fold preference for GluK3 over GluK1 in the present assays, which was less pronounced than previously reported.[9] Furthermore, it is interesting to notice that the unsubstituted QX showed weak affinity (high micromolar K_i) at all recombinant receptors tested.

In the present study, three categories of analogues of compound **1** have been included (Table 1). Among the first series of 6-substituted analogues (**6**, **15** and **18** – **22**), it is clear that smaller-sized substituents, such as CF_3 (**6**), Br (**15**) and I (**18**), all are well accepted at GluK1-3 receptors, with **18** showing similar affinity at GluK3 receptors as compared to compound **1**. The GluK1/GluK2- and GluK1/GluK3-affinity ratios for compounds **6**, **15** and **18** were close to those of compound **1**, indicating a similar trend towards selectivity. However, introduction of alkyne substituents in the 6-position (compounds **19** – **22**) revealed that some of these compounds (except **20**) are well tolerated at GluK3 receptors (K_i's in the range 1-3 μM) and far better tolerated than at GluA2, GluK1 and GluK2 receptors. Interestingly, compound **22** with a phenylethynyl substituent showed a marked GluK3-preference among kainate receptors (GluK1/GluK3- and GluK2/GluK3-affinity

ratios of at least 30), and a GluA2/GluK3-affinity ratio of 8. On the other hand, compound **19** showed a marked 31-fold preference for GluK3 over GluA2, combined with a GluK3 preference over GluK1 (13-fold) and GluK2 (8-fold). Similarly, compound **21** had at least a 100-fold preference for GluK3 over GluA2. The observed affinity ratios indicate that the GluK3 LBD can accept lipophilic and larger-sized ethynyl substituents in the 6-position of the *N*1-substituted quinoxaline-2,3-dione better than GluA2, GluK1 and GluK2.

Secondly, we have synthesized a series of analogues with variation in position 7, including pyrrolyl (**1**), nitro (**12**) and fluoro substituents (**33**) as well as the unsubstituted analogue (**6**). Binding affinities (Table 1) demonstrated that these four compounds have similar preference among the kainate receptors tested and low-micromolar affinities (K_i's in the range 0.2-2.6 μM). Among these compounds, **33** showed the largest GluK3 over GluA2 preference (22-fold).

The major efforts in the present study have been focused on variations at the *N*1-position. Target compounds include one group of compounds (**7** – **12**) with a nitro substituent in position 7, one group (**6**, **24**, **27**) without any substituent in position 7, and finally, a series of target compounds (**32** – **39**) with a fluoro substituent in position 7. The

binding affinity data (Table 1) showed that 7-nitro analogues containing aromatic amido substituents (**12**, benzamido; **7**, *m*-nitrobenzamido and **9**, benzenesulfonamido) all were potent ligands at GluK1, GluK2 and GluK3 receptors with affinities close to those of compound **1**, whereas analogues containing smaller and nonaromatic substituents (**8**, **10**, **11**) were less potent. Of the tested 7-nitro analogues, a similar affinity rank order for compounds **6**, **7**, **9**, **11** and **12** was observed (GluK3 > GluK1 > GluK2 > GluA2). Compound **8** showed a similar rank order at kainate receptors but was found to be weakly GluA2 preferring, whereas the rank order for **10** was GluK3 > GluK2 > GluK1 > GluA2. Compound **24** (with a non-aromatic methylamido substituent in the *N*1-position, but without substituent in position 7) also showed lower affinity at all receptors tested as compared to compound **6**, supporting the observation that aromatic amido substituents are essential in the *N*1-position. Interestingly, compound **27,** having a more flexible phenyl ethyl substituent in the *N*1-position but no amido group, showed a 4-8-fold lower affinity at GluK1, GluK2 and GluK3 receptors as compared to compound **6**, illustrating the importance of having an amido substituent in the *N*1-position. The 7-fluoro analogues (**33** – **39**) were all potent ligands at GluK1, GluK2 and GluK3 receptors with sub- or low

micromolar affinities (K_i's in the range 0.14-4.7 μM), supporting the observation seen above for compound **7** that substitution in the benzamido substituent is allowed. Among the group of compounds (**33** – **39**), compound **37** showed the highest affinity at GluK3 receptors (K_i = 0.142 μM) and similar to that of compound **1** (K_i = 0.187 μM). In addition, compound **37** showed GluK1/GluK3-, GluK2/GluK3- and GluA2/GluK3-affinity ratios of 8, 6 and 29, respectively.

The compounds were also tested in our newly established GluK5 receptor binding assay.[14] CNQX and DNQX possessed the greatest binding affinity at GluK5 (K_i of 8.40 and 7.12 μM, respectively), indicating that GluK5 prefers small antagonists. Among the novel *N*1-substituted quinoxalinediones, compounds **1**, **33** and **37** were the most potent, showing K_i values of 23.9, 30.9 and 26.4 μM, respectively. No distinct structure-affinity relationship could be identified among the novel *N*1-substituted quinoxalinediones when tested at GluK5 homomeric receptors.

Binding affinities for the target compounds were also determined at native NMDA receptors (rat brain synaptosomes) using [^{3}H]-CGP-39653. In the NMDA receptor binding assay, none of the compounds showed substantial affinity (K_i > 10 μM), except for

compound **1** (K_i = 2.53 ± 0.35 μM). Furthermore, the binding affinity of compound **1** to rat brain synaptosomes was also determined using [^{3}H]-kainate. In this assay, compound **1** showed a K_i value of 0.42 ± 0.05 μM. Finally, the binding affinity (K_i) of compound **37** was determined at the ligand-binding domain of GluK1 (GluK1-LBD) to be 113 ± 23 nM, which is 10-fold higher affinity than seen at full-length GluK1. Similar differences between the affinity at full-length GluK1 and GluK1-LBD have previously been observed for other ligands.[15]

In functional pharmacological studies using homomeric GluK1, GluK2 and GluK3 receptors expressed in *X. laevis* oocytes, antagonist affinities (K_b) were measured by TEVC electrophysiology (Figure 2). Compound **1** was confirmed to be an antagonist at GluK1–3 with the calculated K_b values (mean ± SEM, nM): GluK1 = 115 ± 19; GluK2 = 323 ± 27; GluK3 = 50 ± 4.

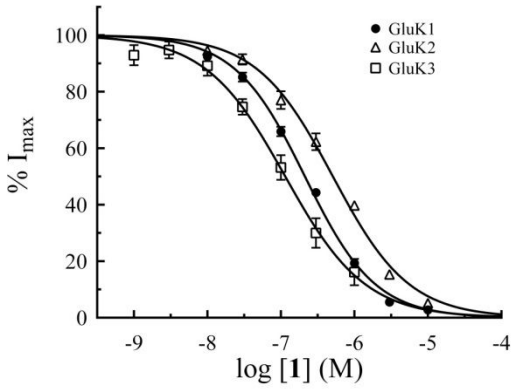

Figure 2. Antagonism by compound **1** (LU 97175) of homomeric kainate receptors. The weakly desensitizing (Cys-Cys)GluK1–3 mutants were expressed in *X. laevis* oocytes and stimulated in duplicate with Glu in the absence or presence of increasing concentrations of **1**. Shown is the mean ± SEM of pooled values from 3–10 oocytes normalized to the control response (absence of antagonist) of each oocyte. The top and bottom of each curve are fixed at 100% and 0%, respectively. K_b (mean ± SEM, nM) = 115 ± 19 (●, GluK1, 10 oocytes); 323 ± 27 (△, GluK2, 6 oocytes); 50 ± 4 (□, GluK3, 3 oocytes). The K_b of GluK2 is statistically significantly different from that of GluK1 and GluK3 ($p < 0.05$, Kruskal-Wallis One Way ANOVA on Ranks with Dunn's post-test). Hill slopes were unity for all curves.

Structural analysis. To obtain information on the detailed binding mode and interactions of this series of compounds, we crystallized GluK1-LBD with **37** as a representative. The reason for selecting **37** was its high affinity at GluK1 combined with its acceptable solubility for crystallization. The X-ray crystal structure of the GluK1-LBD in complex with compound **37** was determined at 1.85 Å resolution and contained one molecule in the asymmetric unit of the crystal (Table 2). This molecule forms a dimer with a symmetry-related molecule (Figure 3A). Binding of **37** led to a domain opening of 33–35° relative to the structure of GluK1-LBD with Glu, which is in the range seen for other antagonists.[15]

Table 2. Crystal data, data collection and structure refinement of GluK1-LBD in complex with compound **37**.

Crystal data	
Space group	*H*32
Unit cell: *a, b*, *c* (Å) α, β, γ (°)	88.87, 88.87, 157.15, 90.0, 90.0, 120.0
Molecules in a.u.[a]	1

Data collection	
Wavelength (Å)	0.97625
Resolution (Å)	37.38-1.85 (1.95-1.85)[b]
No. of unique reflections	20,688 (2,971)
Average redundancy	10.0 (9.6)
Completeness (%)	100 (100)
R_{merge}[c] (%)	8.1 (44.1)
I/σ(I)	6.1 (1.6)
CC1/2	1.00 (0.93)
Wilson B (Å^2)	20.3
Refinement	
R_{work} (%)[d]/R_{free} (%)[e]	18.7/21.6
Amino acid residues/**37**	250/1
Glycerol/sulfate/chloride/water	5/1/1/110
R.m.s. deviation bond length (Å)/angles (°)	0.013/1.1
Average B-values (Å^2) for:	

Amino acid residues/**37**	32.8/21.1
Glycerol/sulfate/chloride/water	77.0/65.2/76.6/33.2
Non-glycine residues in allowed regions of the Ramachandran plot (%)[f]	100

[a] A.u.: asymmetric unit of the crystal. [b] Values in parentheses correspond to the outermost resolution shell. [c] R_{merge} is calculated as follows: $I_i(hkl)$ is the intensity of an individual measurement of the reflection with Miller indices *hkl*, and $I(hkl)$ is the intensity from multiple observations. $R_{merge} = \sum_{hkl}\sum_i|I_i(hkl) - I(hkl)| / \sum_{hkl}\sum_i |I_i(hkl)|$. [d] $R_{work} = \sum_{hkl}|F_{obs} - F_{calc}| / \sum_{hkl} |F_{obs}|$ where F_{obs} and F_{calc} are the observed and calculated structure factor amplitudes, respectively, for reflection *hkl*. [e] R_{free} is equivalent to R_{work}, but calculated with 5% of reflections omitted from the refinement process. [f] The Ramachandran plot was calculated according to MolProbity.[16]

In complex with **37**, the GluK1-LBD forms a compact dimer not previously observed (Figure 3A). Besides the usual interactions between D1 lobes of each subunit comprising the dimer, in the present dimer we also observe tight packing between D2 lobes. This results in a buried surface area at the dimer interface of 1339 Å^2, using the PISA server.[17] The Gly-Thr linker in D2 that substitutes the parts of the receptor protruding to the membrane is in close proximity in the GluK1-LBD dimer with **37**. The Pro667-Pro667 linker-linker distance between the two subunits is 9.7 Å (Figure 3A). The segment Lys544,

Gly-Thr linker and Pro667-Asp673, as well as Thr753-Gly757, is engaged in D2-lobe contacts in the dimer, resulting in a salt bridge being formed between Lys554 of one subunit and Asp673 of the other subunit, and *vice versa* (Figure S1). For comparison, the dimer of GluK1-LBD with the antagonist (*S*)-ATPO (pdb-code 1VSO[18]) has a more common, less compact structure (Figure 3B), resulting in a buried surface area of 1021 $Å^2$ and a linker-linker distance of 20.5 Å. On the other hand, the apex distance measured between Gly771 of each subunit is similar in the GluK1-LBD dimer with **37** (13.7 Å, Figure 3A) and (*S*)-ATPO (12.3 Å; Figure 3B). It seems that this new dimer arrangement of GluK1-LBD is also possible in full-length GluK1, but will require rearrangement of the LBD-transmembrane domain (TMD) linker region (Figure S2). We cannot exclude that the dimer arrangement is an artifact of considering an LBD-construct. However, previous studies on agonists and antagonists have shown that there is a good agreement between the dimer arrangement in the full-length GluA2 receptor and the ligand-binding domain of GluA2 (e.g.[19, 20]). Also, the dimer arrangement could be due to crystal packing contacts, although from comparing crystal packing in different GluK1-LBD structures this is not

obvious as similar regions are predominantly involved in crystal packing despite different surroundings (Figure S3).

Compound **37** could unambiguously be located at the ligand-binding site (Figure 3C). It interacts with residues of lobe D1 (Figure 3C), forming direct hydrogen bonds as previously observed for agonists and antagonists,[15] whereas water-mediated hydrogen bonds only are observed to lobe D2 residues. The 2,3-quinoxazolinedione moiety of **37** interacts with the essential Arg523 in the same manner as previously seen in the structure of GluK1-LBD with compound **2**.[8] Both oxygen atoms of the 2,3-quinoxazolinedione in **37** make hydrogen bonds with Arg523. Furthermore, the 3-one forms a hydrogen bond to the backbone nitrogen atom of Thr518 as well as a dipole-dipole interaction to the side-chain hydroxy group of Thr518. Additionally, the 2-one interacts with a water molecule. The *N*4-nitrogen atom of the 2,3-quinoxazolinedione forms a hydrogen bond to the backbone oxygen atom of Pro516. Pi-pi stacking is observed between the 2,3-quinoxazolinedione moiety and the residue Tyr489 (Figure 3C; distance ~3.7 Å; not shown).

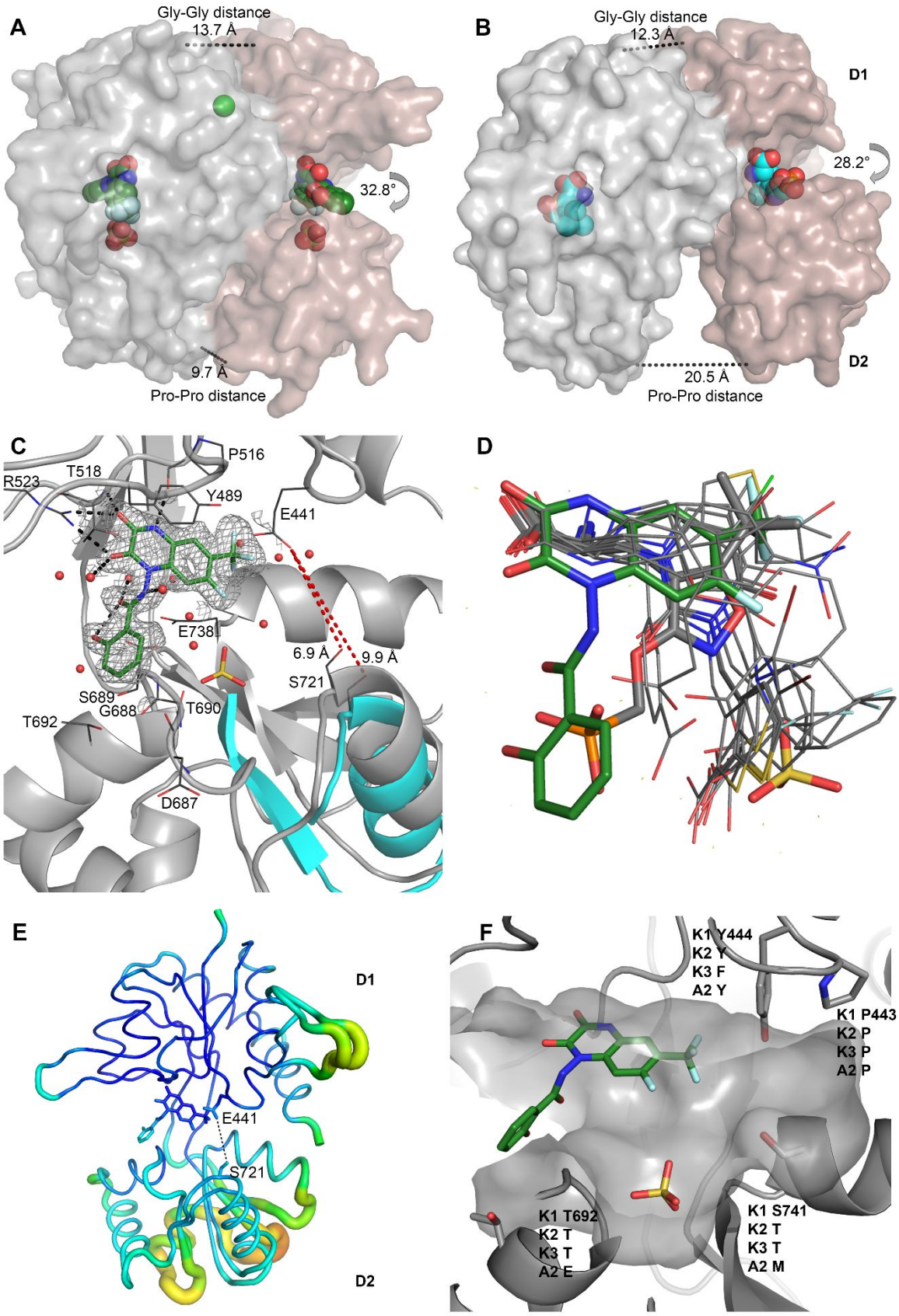
A
Gly-Gly distance
13.7 Å
32.8°
9.7 Å
Pro-Pro distance
B
Gly-Gly distance
12.3 Å
D1
28.2°
D2
20.5 Å
Pro-Pro distance
C
P516
T518
R523
Y489
E441
E738
6.9 Å
9.9 Å
S721
S689
G688
T690
T692
D687
D
E
D1
E441
S721
D2
F
K1 Y444
K2 Y
K3 F
A2 Y
K1 P443
K2 P
K3 P
A2 P
K1 T692
K2 T
K3 T
A2 E
K1 S741
K2 T
K3 T
A2 M

Figure 3. X-ray crystal structure of **37** in GluK1-LBD. (A) The overall conformation of GluK1-LBD dimer (molA grey; symmetry molA dark salmon) is shown in surface representation as well as **37,** sulfate and chloride in spheres representation with carbon atoms in green. The Pro667-Pro667 linker-linker distance between the two subunits is shown as well as the apex Gly771–Gly771 distance and domain opening (arrow). (B) For comparison, the dimer of GluK1-LBD in complex with (*S*)-ATPO (PDB-code 1VSO) is shown as in (A), with (*S*)-ATPO in spheres representation with carbon atoms in cyan. The lobes D1 and D2 are indicated on the figure. (C) Residues forming hydrogen bonds to **37** as well as residues discussed in text are shown as lines with carbon atoms in grey. Potential hydrogen bonds within 3.2 Å are shown as dashed, black lines as well as the distance between Glu441 in lobe D1 and Ser721 in lobe D2 as dashed, red lines. Furthermore, a standard $2F_o$-F_c omit map (grey) contoured at 1 sigma and carved around the ligand at 2.0 Å radius is shown. The protein backbone is shown as cartoon. Alternative conformation of a part of D2 is colored cyan. Oxygen atoms are red, nitrogen atoms blue and sulfur is yellow. Water molecules are displayed as red spheres and the sulfate ion located in the binding site is shown in sticks representation. (D). Superimposition on D1

of all 14 available antagonist structures of rat GluK1-LBD (green sticks: **37** and the binding site sulfate ion; grey sticks: (*S*)-ATPO (1VSO); thin grey lines: PDB-codes 2F34, 2F35, 2OJT, 2QS1, 2QS2, 2QS3, 2QS4, 3S2V, 4DLD, 4QF9, 4YMB, 5M2V). (E). B-factors of the protein reveal a highly dynamic lobe D2. Color range is from blue (10.5 Å) to red (110.8 $Å^2$). One D2 helix is located in two conformations and therefore appears as less flexible. (F) Surface representation to illustrate binding cavity. Residues discussed in text are shown in sticks representation.

The *o*-hydroxy-benzamido substituent at the *N*1 nitrogen atom of **37** has no direct hydrogen bonds to GluK1. In **37**, the phenol ring is positioned in plane with the amide moiety, which allows for an intramolecular hydrogen bond between the carbonyl oxygen of the amide and the hydroxy group. This interaction might reduce the entropy penalty upon binding of **37** at the ligand-binding site. In addition, the amide carbonyl oxygen and the amide nitrogen atom both form a hydrogen bond to a water molecule (Figure 3C).

Pi-pi stacking is observed between the *o*-hydroxy-benzamido substituent and the protein backbone of Gly688–Ser689 (Figure 3C; distance ~3.4 Å).

A sulfate ion is located within 4 Å from the aromatic fluorine atom in **37** (Figure 3C), which forms direct hydrogen bonds to Ser689, Thr690 and Glu738 as well as water molecules. A sulfate ion was also seen at this position in the GluK1-LBD co-crystal structure with compound **2** reported by Demmer *et al,*[8] but not in any of the remaining GluK1 antagonist co-crystal structures.[15] A superposition of **37** and all 13 previously reported rat GluK1-LBD structures with antagonists[15] reveals that **37** occupies a region in the binding site similar to that of (*S*)-ATPO (Figure 3D). Through this binding mode, the *o*-hydroxy-benzamido substituent and the sulfate ion are positioned in the same region of the binding pocket as the phosphonic acid substituent in (*S*)-ATPO, with the phosphonic acid substituent of (*S*)-ATPO positioned in between the hydroxy-benzamido substituent in **37** and the sulfate ion. The phosphonic acid group in (*S*)-ATPO forms hydrogen bonds to the side-chain hydroxy group and backbone nitrogen atom of Ser689 and four water molecules, whereas the hydroxy-benzamido substituent of **37** has no hydrogen bonding interactions with the protein.

The side-chain of Glu738 in D2 is turned away from **37** previously observed.[8, 21] Glu738 is engaged in a hydrogen-bonding network involving Ser689 and Lys762 (not shown). In other GluK1-LBD structures, this residue forms a direct hydrogen bond with agonists and antagonists containing an amino acid moiety.[15]

The D2 residues 718-736, as well as the D1 loop comprising residues 450-455 and forming crystal packing contacts to 718-736, were built in two alternative conformations (altA and altB; Figure S5). The altA position of the helix (718-728) is seen in other structures with antagonists, whereas altB might be considered unusual. As the buried surface area of the segment 718-736 in altB is larger (970 $Å^2$) compared to altA (852 $Å^2$), it might contribute to stabilize the altB position. For comparison, the size of the buried surface area of 718-736 is 909 $Å^2$ for GluK1-LBD with (*S*)-ATPO. AltA and altB also lead to small differences in the calculated domain opening: 33° and 35°, respectively. These domain openings are approximately 6° larger than the domain opening stabilized by (*S*)-ATPO (28°).

There seems to be a tendency that GluK1-LBD structures with antagonists reveal more flexibility in the D2 lobe than observed for structures of complexes with agonists (with full

domain closure) (Figure S4). High B-values are seen in lobe D2 in the structure of GluK1-LBD with **37** (Figure 3E). This lobe D2 flexibility might be explained by the loss of D1-D2 interlobe contacts. One such important contact is the hydrogen bond from the side-chain carboxylate group of Glu441 to the side-chain hydroxy group of Ser721.[15] Ser721 is positioned at the *N*-terminal end of a helix that has been modeled in two different conformations (Figure 3C). This leads to a distance of 6.9 Å between the side-chain carboxylate oxygen atom in Glu441 and the hydroxy group in Ser721 in one helix conformation (altA) and 9.9 Å in the other helix conformation (altB). Thus, the large domain opening leads to loss of a potential hydrogen bond compared to structures with agonists.

Structure-affinity relationships. Combining the observed structure-affinity relationships included in the present study (Table 1) with the GluK1-LBD co-crystal structure of compound **37** gives rise to important points. As detailed in the pharmacology section, several of the compounds with substituents in position 6 such as trifluoromethyl (**6**), bromo (**15**), iodo (**18**) and the smaller alkynyl substituents (**19** and **21**) are accepted at GluK1 (K_i's in the range 1.3-15.9 μM), GluK2 (K_i's in the range 2.0-9.8 μM) and GluK3

receptors (K_i's in the range 0.4-1.2 μM). From the co-crystal structure of compound **37** it is apparent that with an assumed binding conformation similar to that of **37,** these substituents are accommodated in the region of Tyr444 and Ser741 in GluK1 receptors (Figure 3F). Inspecting the crystal structure, it is observed that 6-substituents containing a triple bond (compounds **19** – **22**) would extend towards Tyr444. The flexible part of the 6-substituent in **19** and **21** would be able to bend away, avoid steric clash with Tyr444 and perhaps make potential hydrogen bonds to Ser741 or in the area of Tyr444. However, substituents in position 6 with more steric bulk and less flexibility as in **20** and **22** cannot be accommodated in GluK1 (K_i >100 μM) most likely due to steric clash with Pro443 and Tyr444. At GluK2, neither compound **20** nor **22** show affinity, whereas compound **22** containing a 2-phenyl-ethynyl substituent possesses low-micromolar affinity at GluK3 (K_i = 2.91 μM; Table 1).

To address the difference in binding affinities of the three alkynyl target compounds (**19**, **21** and **22)** at GluK1 and GluK3, we have constructed a simple model of the LBD of GluK3 and used this together with the GluK1-LBD co-crystal structure to explain the differences in binding affinities of selected compounds (Figure 4). The GluK3-LBD model, having

Phe446, Ala691 and Thr742 instead of GluK1 Tyr444, Ser689 and Ser741, has the same open conformation as seen in the present GluK1-LBD structure in complex with compound **37** allowing binding of antagonists. The Ser689 to Ala691 modification close to the *N*1-benzamido substituent is not expected to have a major effect on this region of the receptor, as Ser689 in the GluK1 structure points its polar side chain part away from the *N*1-benzamido substituent. However, the Tyr444 to Phe446 modification is likely to lead to more spacious and less hydrophilic surroundings in GluK3 as compared to GluK1 due to difference in size. Phe446 of GluK3 will not be able to contribute to the hydrogen bonding network observed in the GluK1-LBD crystal structure connecting the side chains of Tyr444 and Ser741 (as well as Thr740) through two water molecules (Figure 4A).

When compounds **19** and **21** are introduced in the GluK1-LBD structure, the alkynyl substituents are likely to get into too close contact with Tyr444, or the alkynyl substituents will displace the two water molecules and therefore interfere with the hydrogen bonding network connecting Tyr444 with Ser721, which could explain the 14- and 11-fold reduction in affinity at GluK1, respectively, as compared to compound **37**. When compounds **19** and **21** are introduced in the GluK3-LBD model (Figure 4B), the alkynyl

substituents may be better accommodated due to the presence of Phe446, and the hydroxy groups of **19** and **21** may engage in hydrogen bonding interactions with Thr742. The differences described are likely to contribute to the 8-fold reduction in affinity at GluK3 for compounds **19** and **21** as compared to compound **37**.

When compound **22** with a longer, larger and non-polar alkynyl substituent is introduced, the alkynyl substituent is also likely to get into too close contact with amino acid residues such as Tyr444 of GluK1. Additionally, this compound may, because of lack of polar groups, to a larger extent than compounds **19** and **22** interfere with the hydrogen-bonding network seen in the GluK1-LBD structure, thus reflecting the observed lack of affinity (K_i > 100 μM). In contrast, in the GluK3-LBD model it is hypothesized (Figure 4C), that the alkynyl side chain of **22** may be accommodated between Phe446 and Thr742 in more lipophilic surroundings, created by a possible rotation of the Thr742 polar side chain to avoid steric clash with the substituent of **22** and to provide hydrophobic interactions. We believe these differences between GluK1 and GluK3 receptors contribute to the explanation of the observed GluK3 preference of compound **22** over GluK1 receptors.

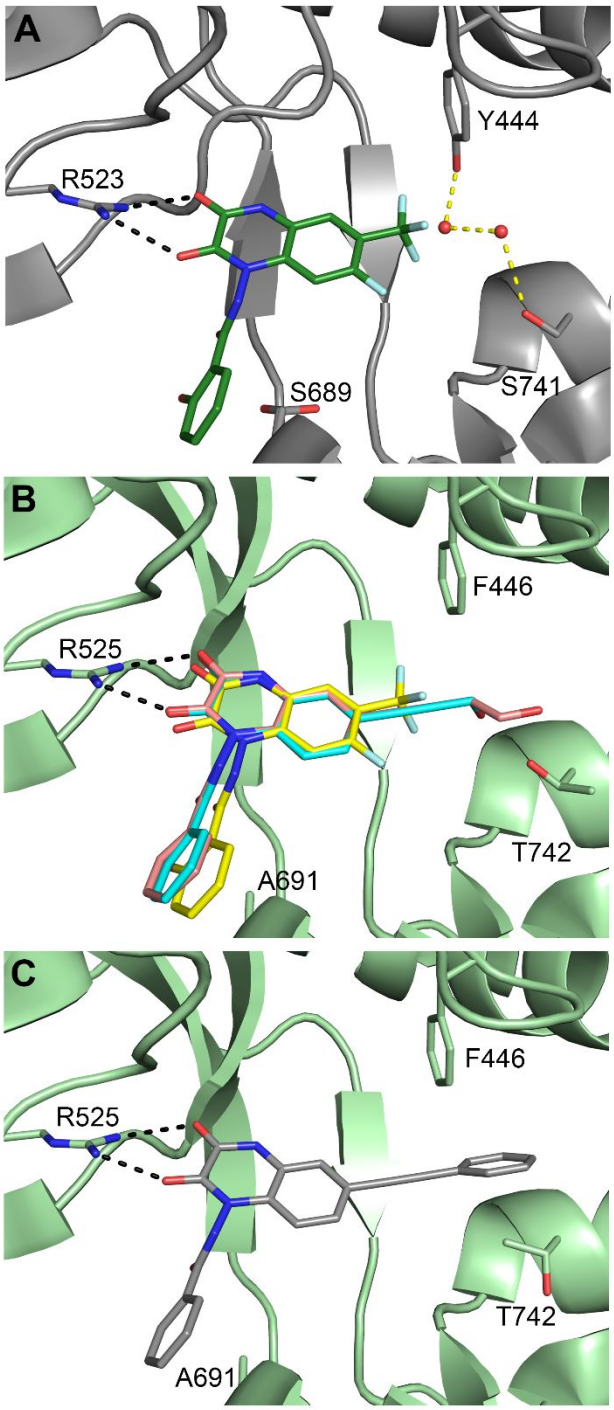

Figure 4. A simple model of GluK3-LBD in an open conformation superposed on GluK1-LBD in complex with **37**. The proteins are shown in cartoon representation (GluK1-LBD

in grey, GluK3-LBD in palegreen). Residues mentioned in the text are shown in sticks, coloured according to the protein. Hydrogen bonds to Arg523/525 (GluK1/GluK3 numbering) are shown as black dashed lines. (A) GluK1-LBD crystallized in complex with **37**. Compound **37** is shown in green sticks. Water molecules are shown as red spheres. Water mediated hydrogen bonds are shown as yellow dashed lines. (B) Modelled ligands into GluK3-LBD are shown in sticks: **19** in cyan, **21** in salmon, and **37** in yellow. (C) Compound **22** (grey) modelled into GluK3-LBD.

From the GluK1 and GluK3 binding data, it is clear that analogues with larger aromatic substituents at *N*1, such as benzamido, (e.g. **37**, K_i = 1.12 μM at GluK1 and 0.142 μM at GluK3, Table 1) in general are more favorable than smaller non-aromatic groups (see e.g. **32** with *N*1-amino group and 7-fluoro (K_i = 12.6 μM at GluK1 and 5.24 μM at GluK3), **24** with *N*1-acetamido and 7-hydrogen (K_i = 17.4 μM at GluK1 and 8.83 μM at GluK3) and **10** with *N*1-(*N*-acetylacetamido) and 7-nitro (K_i = 36.8 μM at GluK1 and 5.97 μM at GluK3)). This observation is consistent with the idea that the benzamido moiety reaches

into an area of the receptor where additional steric bulk is allowed in both GluK1 (Figure 3F) and GluK3.

Substitution is allowed at the benzamido ring (hydroxy, methoxy and nitro groups), with a hydroxy group in the *meta* position (**38**, K_i = 0.80 μM at GluK1 and 0.329 μM at GluK3) leading to the same affinity as the unsubstituted compound (**33**, K_i = 0.802 μM at GluK1 and 0.277 μM at GluK3). The *m*-hydroxy group would be able to interact with the side-chain hydroxy group of Thr692 in GluK1-LBD, whereas a *p*-hydroxy group (**39**) could interact with the side-chain hydroxy group of Thr692 and the backbone carbonyl oxygen atom of Asp687 (Figure 3C,F). Similar interactions would be possible in GluK3. Compounds **33** and **38** show a more than 7-fold preference towards the kainate receptors (GluK1-3) over the AMPA receptor GluA2. This preference might be explained by the differences in residues in the vicinity of the benzamido substituent where the conserved Thr692 of the kainate receptors correspond to Glu in GluA2 (Figure 3F).

Some of the target compounds, such as **6**, **9**, **12** and **27,** were designed to address the importance of the *N*1-benzamido part. Even though none of these compounds contains an *o*-hydroxy substituent in the aromatic part and thus are not able to achieve

intramolecular stabilizations through intramolecular hydrogen bonding as is seen for compound **37**, the X-ray structure of compound **37** in GluK1-LBD shows that the benzamido carbonyl oxygen forms a hydrogen bond through water to the side chain ammonium group of of Lys762. Such hydrogen bonding most likely also occurs for compounds **6** and **12** (both containing an *N*1-benzamido part) as well as for compound **9** (containing an *N*1-benzensulphonamido part). However, similar hydrogen bonding to the side-chain ammonium group of Lys762 through a water molecule is not possible for compound **27** (containing a flexible ethyl-spacer between *N*1 and the aromatic part of the substituent). These observations could explain the 5-10 fold reduced affinity seen for compound **27** as compared to **6**, **9** and **12** in the GluK1, GluK2 and GluK3 receptor binding assay.

CONCLUSION

Based on the observation that *N*1-substituted reference quinoxaline-2,3-dione (such as compound **1**, LU 97175) showed preference for recombinant kainate receptors over

AMPA receptors,[9] we have synthesized 23 new analogues in order to investigate the structure-affinity relationships. Binding affinities were determined at recombinant AMPA and kainate receptors, including the newly established assay on GluK5. The major efforts in the present study were focused on variations at the *N*1-position and 6-position. Aromatic amido substituents were essential in the *N*1-position, while smaller-sized substituents were preferred in 6-substituted analogues. Four of the new compounds (**19**, **21**, **22** and **37**) showed notable preference for the GluK3 receptor over GluK1 and GluK2. Introduction of alkyne substituents in the 6-position were generally well tolerated at GluK3 receptors in contrast to at GluA2, GluK1 and GluK2 receptors, with compound **22** showing a marked GluK3-preference (GluK1/GluK3- and GluK2/GluK3-affinity ratios of at least 30). Compound **19** showed 31-fold preference for GluK3 over GluA2, combined with a GluK3 preference over GluK1 (13-fold) and GluK2 (8-fold). Compound **21** had at least a 100-fold preference for GluK3 over GluA2 combined with an 11-fold preference for GluK3 over GluK1. Compound **37** containing an *o*-hydroxy-benzamido in the *N*1-position and CF_3 in the 6-position showed the highest binding affinity at GluK3 receptors with GluK1/GluK3-, GluK2/GluK3- and GluA2/GluK3-affinity ratios of 8, 6 and 29, respectively. Compound **37** was crystallized in complex with the ligand-binding domain of GluK1 and induced a domain opening comparable to other antagonists.

In complex with **37**, the GluK1-LBD formed a compact dimer not previously observed where both lobes D1 and D2 were engaged in dimer formation. This structure-activity study, combined with structural information from crystallizing the ligand-binding domain of GluK1 with a representative from this series of new compounds, might aid future design of GluK3 preferring compounds.

METHODS

Chemistry. General. Commercially available chemicals were used without any purification. Anhydrous reactions were carried out in oven or flame dried glassware. Dry solvents (DMF, THF and DCM) were dried using a solvent purification system. Thin layer chromatography was performed on TLC silica gel 60 F_{254} and compounds were visualized using UV light (254 nm). For flash column chromatography Merck silica gel 60 (0.063–0.200 mm) was used as the stationary phase. LC-MS was performed at an Agilent 1100 HPLC with an XBridge 3.5 μm C-18 column (100 × 4.6 mm) using a linear gradient elution from buffer A (H_2O:MeCN:HCOOH, 95:5:0.1) to buffer B (H_2O:MeCN:HCOOH, 5:95:0.1)

over 10 min. Flow rate: 1.0 mL/min. The HPLC was coupled to a Hewlett Packard 1100 series mass spectrometer with an electrospray ionization source. Preparative HPLC was carried out on a Dionex ultimate 3000 system with binary pump, UV/VIS detector and 10 mL injection loop. The column was a Gemini® 5 µm NX-C18 110 Å, LC Column 250 × 21.2 mm. Appropriate linear gradient programs were set up using mobile phase A (H_2O:HCOOH, 100:0.1) and mobile phase B (H_2O:MeCN:HCOOH, 10:90:0.1) with a flow rate of 15 mL/min. The following UV wavelengths were monitored: 200, 254 and 290 nm. ^{1}H-NMR was performed on a 400 MHz Bruker Avance III equipped with a 5 mm broad band probe at 400.09 MHz. Samples were dissolved in DMSO-d_6 and analyzed at 300 K. Proton spectra were acquired with 16–32 scans collecting 32k data points which were transformed to 64k and referenced using DMSO-d_6 at 2.500 ppm. ^{13}C-NMR was performed at 100.61 MHz with 1024–3072 scans (depending on the concentration) using DMSO-d_6 at 39.510 ppm as reference. Elemental analysis was recorded on a Perkin Elmer 2400 CHN Elemental Analyzer and performed by the Department of Physical Chemistry at the University of Vienna in Austria.

Synthesis of target compound 37 and related intermediates

1,5-Dichloro-2-nitro-4-(trifluoromethyl)benzene (29). KNO_3 (49.5 g, 490 mmol) was added portionwise over 30 min at 15 °C to a stirred suspension of 1,3-dichloro-4-(trifluoromethyl)benzene, **28,** (95.77 g, 445 mmol) in conc. H_2SO_4 (400 mL). The stirring was continued for 18 h at rt. The reaction mixture was poured into ice water (1500 g) and extracted with diethylether (1 × 600 mL + 1 × 200 mL). The combined organic layers were washed with sat. $NaHCO_3$ (100 mL) and brine (200 mL) and dried over Na_2SO_4 and concentrated *in vacuo*. The residue was purified by recrystallization (petroleum ether bp 40–60 °C) to afford **29** as a yellow solid (100.6 g, 87%). ^{1}H NMR δ 8.56 (s, 1H), 8.35 (s, 1H). ^{13}C NMR δ 146.48, 136.16 (q, *J* = 1.7 Hz), 134.99, 131.34, 127.02 (q, *J* = 32.8 Hz), 125.78 (q, *J* = 5.5 Hz), 121.94 (q, *J* = 273.7 Hz).

1,5-Difluoro-2-nitro-4-(trifluoromethyl)benzene (30). Potassium fluoride (44.7 g, 770 mmol) was dried in a 250 mL round bottom flask by heating it to 140 °C in an oil bath for 2 h in high vaccum with magnetical stirring. After cooling to rt, dry DMF (100 mL) and compound **29** (50.0 g, 192 mmol) were added and the reaction mixture heated to 160 °C for 1 h 45 min. The temperature was increased to 170 °C for 30 min. The reaction mixture was diluted with diethyl ether (200 mL) and filtered. The solids were washed with diethyl

ether (100 mL) till colorless. The combined organic layers were washed with brine (2 × 100 mL + 4 × 50 mL). The organic layer was dried ($MgSO_4$), filtered and concentrated *in vacuo*. The crude product was distilled through a 20 cm Vigreux column at 57–58°C (1.6–1.7 mbar) to afford **30** as a yellowish liquid (34.64 g, 79%). ^{1}H NMR δ 8.55 (t, *J* = 7.6 Hz, 1H), 8.09 (t, *J* = 10.8 Hz, 1H). ^{13}C NMR δ 164.01–160.86 (m), 158.73 (dd, *J* = 270.5, 14.3 Hz), 134.38 (d, *J* = 7.6 Hz), 126.57 (p, *J* = 4.5 Hz), 126.05–117.24 (m), 114.38 (qdd, *J* = 34.7, 14.4, 4.2 Hz), 109.76 (t, *J* = 26.3 Hz).

***tert*-Butyl 2-(5-Fluoro-2-nitro-4-(trifluoromethyl)phenyl)hydrazine-1-carboxylate (31)**. *tert*-Butyl hydrazinecarboxylate (5.0 g, 37.8 mmol) was added to a stirred solution of compound **30** (7.81 g, 34.4 mmol) in dry DMSO in an atmosphere of N_2. The reaction was stirred at 0 °C for 2 min and at rt for 30 min. The reaction mixture was then poured into 0.1% aqueous $NaHCO_3$ (1500 mL) and stirred for 30 min. The yellowish precipitate was filtered, washed with H_2O and dried *in vacuo* to give **31** as a yellow solid (11.42 g, 98%). ^{1}H NMR δ 9.90 (br s, 1H), 9.46 (br s, 1H), 8.40 (d, *J* = 7.3 Hz, 1H), 7.02 (d, *J* = 13.5 Hz, 1H), 1.45 (s, 9H). ^{13}C NMR δ 163.12 (dq, *J* = 256.0, 2.4 Hz), 155.35, 150.71 (d, *J* = 13.0 Hz), 127.80 (q, *J* = 5.0 Hz), 127.52, 122.42 (q, *J* = 271.67 Hz), 105.94 (qd, *J* = 34.5, 16.3

Hz), 101.99 (d, *J* = 27.5 Hz), 80.72, 28.43. LCMS t_R = 7.226 min $[M+H-C_4H_{10}]^+$ = 284.0; $[M+H-BOC]^+$ = 239.9.

1-Amino-7-fluoro-6-(trifluoromethyl)-1,4-dihydroquinoxaline-2,3-dione (32). Compound **31** (11.40 g, 33.6 mmol) and 5% Pd/C (0.851 g) were mixed in 160 mL 99.98% EtOH. The reaction mixture was hydrogenated in a Parr hydrogenation apparatus at 60 psi for 17 h. Hereafter, the reaction mixture was filtered through Celite, washed with 99.98% EtOH and concentrated *in vacuo*. 1,2-Dichlorobenzene (600 mL) and oxalyl chloride (2.97 mL, 35.1 mmol) were added and the reaction mixture was stirred for 1 h at 130 °C. The reaction mixture was filtered while hot and the solid was washed with cooled ether. The filtrate was concentrated *in vacuo* and purified by column chromatography (AcOEt:Hep:AcOH) to afford **32** as a white/yellow solid (2.878 g, 34%). ^{1}H NMR δ 12.23 (br s, 1H), 7.64 (d, *J* = 12.2 Hz, 1H), 7.46 (d, *J* = 6.6 Hz, 1H), 5.86 (br s, 2H). ^{13}C NMR δ 154.97, 154.96 (dq, *J* = 246.8, 2.2 Hz), 153.78, 133.27 (d, *J* = 11.0 Hz), 127.08–118.79 (m), 113.60 (qd, *J* = 7.1, 2.3 Hz), 111.08 (qd, *J* = 33.2, 14.5 Hz), 104.02 (d, *J* = 27.9 Hz). LCMS t_R = 5.390 min $[M+H]^+$ = 264.0. Elemental analysis (%) calculated for $C_9H_5F_4N_3O_2$: C 41.08, H 1.92, N 15.97. Found: C 41.40, H 1.76, N 15.29.

***N*-(7-Fluoro-2,3-dioxo-6-(trifluoromethyl)-3,4-dihydroquinoxalin-1(*2H*)-yl)-2-methoxybenzamide (34)**. To compound **32** (550 mg, 2.09 mmol), partly dissolved in chlorobenzene (55 mL), 2-methoxybenzoyl chloride (464 mg, 2.72 mmol) was added and the reaction mixture was stirred for 3 days at 135 °C. AcOEt (70 mL) was added and the organic layer was washed with water (2 × 70 mL). The organic layer was dried with Na_2SO_4 and concentrated *in vacuo*. The residue was purified in 15 mg injections using preparative HPLC. Appropriate fractions were concentrated and freeze dried to give **34** as a white solid (433 mg, 52%). ^{1}H NMR δ 12.47 (br s, 1H), 11.24 (br s, 1H), 7.78 (dd, *J* = 7.5, 1.8 Hz, 1H), 7.63 (td, *J* = 8.4, 1.8 Hz, 1H), 7.57 (d, *J* = 6.5 Hz, 1H), 7.46 (d, *J* = 11.7 Hz, 1H), 7.28 (dd, *J* = 8.4, 1.0 Hz, 1H), 7.14 (td, *J* = 7.5, 1.0 Hz, 1H), 3.99 (s, 3H). ^{13}C NMR δ 164.83, 157.87, 155.22 (d, *J* = 245 Hz), 153.80, 153.66, 134.08, 133.28 (d, *J* = 10.6 Hz), 130.98, 122.76 (q, *J* = 272.2 Hz), 121.54 (d, *J* = 2.2 Hz), 121.23, 120.98, 114.54, 112.83, 112.04 (d, *J* = 14.1 Hz), 103.60 (d, *J* = 28.2 Hz), 56.58. LCMS t_R = 6.03 min $[M+H]^+$ = 398.0. Elemental analysis (%) calculated for $C_{17}H_{11}F_4N_3O_4$: C 51.40, H 2.79, N 10.58. Found: C 51.19, H 2.68, N 10.59.

***N*-(7-Fluoro-2,3-dioxo-6-(trifluoromethyl)-3,4-dihydroquinoxalin-1(*2H*)-yl)-2-hydroxybenzamide (37).** A mixture of compound **34** (250 mg, 0.629 mmol) and piperazine (163 mg, 1.89 mmol) in DMA (5 mL) was stirred at 150 °C in an atmosphere of N_2 for 8 h. The reaction mixture was purified in 30 mg injections using preparative HPLC. Appropriate fractions were concentrated and freeze dried to afford **37** as a white solid (95 mg, 39%). ^{1}H NMR δ 12.47 (br s, 1H), 11.38 (br s, 2H), 7.88 (dd, *J* = 7.8, 1.7 Hz, 1H), 7.59–7.45 (m, 3H), 7.06 (dd, *J* = 5.6, 0.6 Hz, 1H), 7.01 (dd, *J* = 5.0, 0.7 Hz, 1H). ^{13}C NMR δ 166.35, 158.05, 155.32 (d, *J* = 248.1 Hz), 153.76, 134.75, 133.35 (d, *J* = 10.7 Hz), 130.58, 122.7 (q, *J* = 272.0 Hz), 121.48 (d, *J* = 2.1 Hz), 119.85, 117.48, 116.74, 114.44 (q, *J* = 4.9 Hz), 112.21 (dq, *J* = 33.4, 14.4 Hz), 103.78 (d, *J* = 28.1 Hz). Elemental analysis (%) calculated for $C_{16}H_9F_4N_3O_4 \cdot 1.5\ H_2O$: C, 46.84; H 2.95, N 10.24. Found: C 46.81, H 2.78, N, 10.08.

Receptor binding studies. Binding at native iGluRs in rat brain synaptosomal membranes was carried out as previously detailed.[22] Ligand affinities at recombinant rat homomeric GluA2 and GluK1-3 and mouse homomeric GluK5 as well as GluK1-LBD were determined as previously described.[23, 24] [^{3}H]-AMPA was used as the radioligand

for GluA2 and [^{3}H]-kainate used for GluK1,2,3,5. The newly developed radioligand [^{3}H]-NF608[25] was used for GluK1-LBD binding experiments and also some GluK1 competition experiments. Competition curves ($n \geq 3$) were conducted in triplicate at 12–16 ligand concentrations. Data were analyzed using GraphPad Prism 6 (GraphPad Software, San Diego, CA) to determine ligand affinity (K_i- one site equation) and Hill slope (4-parameter logistic equation) values.

Functional pharmacology. Antagonist affinity (K_b) of **1** was measured by TEVC electrophysiology using the weakly desensitizing homomeric (Cys-Cys) GluK1,2,3 mutants[26] expressed in *X. laevis* oocytes as previously detailed[27]. Glu concentrations (CC-GluK1, 100 μM; CC-GluK2, 100 μM; CC-GluK3, 10 mM) near the respective EC_{50} value (CC-GluK1, 83.5 μM; CC-GluK2, 108 μM; CC-GluK3, 9.03 mM) were used. Stimulations were conducted in duplicate at each antagonist concentration and converted to % control response before data pooling. Data were analyzed using GraphPad Prism 6 (GraphPad Software, San Diego, CA) to determine ligand affinity (K_i- one site equation) and Hill slope (4-parameter logistic equation) values.

X-ray structure determination. The rat GluK1-LBD (GluR5-S1S2[28]) was expressed and purified essentially as previously described.[28] GluK1-LBD in complex with **37** was crystallized using the hanging drop vapor diffusion method at 7 °C. The drop contained 1 µL of the complex solution (4.0 mg/mL GluK1-LBD and 1.4 mM **37** in 10 mM HEPES pH 7.0, 20 mM sodium chloride and 1 mM EDTA) and 1 µL of reservoir solution (20% PEG4000, 0.1 M lithium sulfate and 0.1 M sodium acetate pH 5.5). Reservoir volume was 0.5 mL. The crystals appeared within one week, and they were flash cooled in liquid nitrogen after soaking in cryo buffer consisting of the reservoir solution with 20% glycerol added. X-ray data of the GluK1-LBD in complex with **37** were collected at the ID23-1 beamline (ESRF, Grenoble, France) at a wavelength of 0.97625 Å to 1.85 Å resolution. Data processing was performed with XDS[29] and SCALA within the CCP4i suite of programs.[30]

The structure determination was carried out using molecular replacement and the program PHASER[31] implemented in CCP4i. The GluK1-LBD with an antagonist (PDB-code 4QF9, molA[8] divided into D1 and D2) was used as a search model, including protein atoms only. A solution was found, showing one molecule in the asymmetric unit

of the crystal. AutoBuild in PHENIX[32] was initially used. Coordinates of **37** were created in Maestro [Maestro version 10.7 Schrödinger, LLC, New York, NY, 2016], geometry optimized [MacroModel 11.3, Schrödinger, LLC, New York, NY, 2016]) and fitted unequivocally into the electron density. Ligand restraint file for **37** was generated using eLBOW[33], keeping the geometry. The structure was refined in PHENIX using individual isotropic B-values, TLS and riding hydrogen atoms. Between refinement steps, the structure was inspected and corrected in COOT[34] and missing residues were built into the structure, except the *N*-terminal residues Gly-Ala-Asn431 and the *C*-terminal residues Gly801, Asn802, Gly803, Cys804 and Pro805. Gradually, sulfate, chloride, glycerol and water molecules were manually modeled into the electron densities. The structure was validated using tools in PHENIX and COOT. For statistics on data collection and refinements, see Table 2.

Domain opening of GluK1-LBD in complex with **37**, relative to the structure of GluK1-LBD with Glu (PDB-code 2F36, molA),[35] was calculated using the DynDom Server.[36] Figures were prepared in PyMOL [The PyMOL Molecular Graphics System, version 1.5.0.5, Schrödinger, LLC].

Construction of GluK3-LBD model. A simple model of GluK3-LBD in an open conformation was constructed using the closed structure of GluK3-LBD in complex with Glu (pdb-code 4MB5; GluK3-LBD_{closed}) and the present open structure of GluK1-LBD in complex with compound **37** as reference (GluK1-LBD_{open}). GluK3-LBD_{closed} was divided into the two lobes D1 and D2. The individual D1 and D2 lobes of GluK3-LBD_{closed} were superimposed on corresponding D1 and D2 lobes in GluK1-LBD_{open} using COOT. This resulted in a model of GluK3-LBD in an open cleft conformation (GluK3-LBD_{open}). The residues in the D1-D2 linker regions were manually rebuilt to optimize geometry. The four ligands, **19**, **21, 22** and **37**, were built in Maestro and geometry optimized in MacroModel, followed by a conformational search for low energy conformations. The different ligands were placed in the binding pocket of GluK3-LBD_{open}, based on the binding mode observed for compound **37** in GluK1-LBD_{open}. Small adjustments of torsion angles in the ligands were performed to avoid steric clashes with residues of the protein and still preserving hydrogen bonds to essential residues of the binding pocket. In addition, the conformation of one side chain in GluK3-LBD_{open} was changed: Thr742 in order to avoid steric clash with **22** and to have a hydrophobic interaction.

ASSOCIATED CONTENT

Supporting Information.

The Supporting Information available free of charge on the ACS Publication website at DOI: XXX, includes

Synthesis and characterization of compounds; Figure S1, Dimer interactions; Figure S2, Comparison of new dimer with full-length structure; Figure S3, Crystal packing contacts; Figure S4, B-factors; Figure S5, Two alternative conformations of residues 718-736 and 450-455 (PDF)

Accession Codes

The structure coordinates and corresponding structure factor file of GluK1-LBD with **37** has been deposited in the Protein Data Bank under the accession code 6FZ4.

AUTHOR INFORMATION

Corresponding Authors

* For T.N.J.: E-mail: tnj@sund.ku.dk. Phone: +45 35336412.

* For K.F.: Corresponding author on crystallography. E-mail: Karla.frydenvang@sund.ku.dk. Phone: +45 35336207.

* For D.S.P.: Corresponding author on pharmacology. Email: picker@sund.ku.dk Phone: +45 35334342.

Present Addresses

†For J.B.: LEO Pharma A/S, Industriparken 55, DK-2750 Ballerup, Denmark

Author Contributions

Design and synthesis: J.P., J.B. and T.N.J. Pharmacology: B.N., D.P., L.H., L.M. and D.S.P. Crystallography and in silico modeling: S.M., K.F. and J.S.K. All authors interpreted data and contributed to data analysis. All authors wrote the manuscript. All authors have given approval to the final version of the manuscript.

Funding

This research was generously supported by the Lundbeck Foundation (Møllerud, Pickering, Frydenvang, Kastrup), Novo Nordisk Foundation (Kastrup), GluTarget (Bornholdt, Johansen), Danscatt (Møllerud, Frydenvang, Kastrup), CoNeXT (Kastrup), BioStruct-X (Møllerud, Frydenvang, Kastrup).

Notes

The authors declare no competing financial interests.

ACKNOWLEDGMENT

Heidi Peterson is thanked for help with expression and purification of the ligand-binding domain of GluK1. ESRF, Grenoble, France is thanked for providing beamtime.

ABBREVIATIONS USED

GluK1-LBD, ligand-binding domain of GluK1; iGluRs, ionotropic glutamate receptors; LBD, ligand-binding domain; TEVC, two electrode voltage clamp. (*S*)-ATPO, (*S*)-2-amino-3-[5-*tert*-butyl-3-(phosphonomethoxy)-4-isoxazolyl]propionic acid; CNQX, 7-nitro-2,3-dioxo-1,4- dihydroquinoxaline-6-carbonitrile; DIPEA, *N,N*-diisopropylethylamine; DNQX,

6,7-dinitroquinoxaline-2,3-dione; LU 97175, 1-benzamido-7-pyrrol-1-yl-6-trifluoromethyl-quinoxaline-2,3-(1*H*,4*H*)-dione; LY 466195, (3*S*,4*aR*,6*S*,8*aR*)-6-(((2*S*)-2-carboxy-4,4-difluoro-1-pyrrolidinyl)methyl)decahydro-3-isoquinolinecarboxylic acid; NBQX, 2,3-dioxo-6-nitro-1,2,3,4-tetrahydrobenzo[*f*]quinoxaline -7-sulfonamide; [^{3}H]NF608, (*S*)-2-amino-3-(6-[^{3}H]-2,4-dioxo-3,4-dihydrothieno[3,2-d]pyrimidin-1(2*H*)-yl)propanoic acid; QX, 1,4-dihydroquinoxaline-2,3-dione; TEA, triethylamine; UBP310, (*S*)-1-(2-amino-2-carboxyethyl)-3-(2-carboxy-thiophene-3-yl-methyl)-5-methylpyrimidine-2,4-dione.

REFERENCES

(1) Traynelis, S. F., Wollmuth, L. P., McBain, C. J., Menniti, F. S., Vance, K. M., Ogden, K. K., Hansen, K. B., Yuan, H., Myers, S. J., and Dingledine, R. (2010) Glutamate receptor ion channels: structure, regulation, and function, *Pharmacol. Rev. 62*, 405-496.

(2) Chang, P. K., Verbich, D., and McKinney, R. A. (2012) AMPA receptors as drug targets in neurological disease--advantages, caveats, and future outlook, *Eur. J. Neurosci. 35*, 1908-1916.

(3) Lemoine, D., Jiang, R., Taly, A., Chataigneau, T., Specht, A., and Grutter, T. (2012) Ligand-gated ion channels: new insights into neurological disorders and ligand recognition, *Chem. Rev. 112*, 6285-6318.

(4) Bleakman, D., Alt, A., and Nisenbaum, E. S. (2006) Glutamate receptors and pain, *Semin. Cell Dev. Biol. 17*, 592-604.

(5) Lerma, J., and Marques, J. M. (2013) Kainate receptors in health and disease, *Neuron 80*, 292-311.

(6) Carta, M., Fievre, S., Gorlewicz, A., and Mulle, C. (2014) Kainate receptors in the hippocampus, *Eur. J. Neurosci. 39*, 1835-1844.

(7) Jane, D. E., Lodge, D., and Collingridge, G. L. (2009) Kainate receptors: pharmacology, function and therapeutic potential, *Neuropharmacology 56*, 90-113.

(8) Demmer, C. S., Møller, C., Brown, P. M., Han, L., Pickering, D. S., Nielsen, B., Bowie, D., Frydenvang, K., Kastrup, J. S., and Bunch, L. (2015) Binding mode of an alpha-amino acid-linked quinoxaline-2,3-dione analogue at glutamate receptor subtype GluK1, *ACS Chem. Neurosci. 6*, 845-854.

(9) Löscher, W., Lehmann, H., Behl, B., Seemann, D., Teschendorf, H. J., Hofmann, H. P., Lubisch, W., Hoger, T., Lemaire, H. G., and Gross, G. (1999) A new pyrrolyl-quinoxalinedione series of non-NMDA glutamate receptor antagonists: pharmacological characterization and comparison with NBQX and valproate in the kindling model of epilepsy, *Eur. J. Neurosci. 11*, 250-262.

(10) Demmer, C. S., Rombach, D., Liu, N., Nielsen, B., Pickering, D. S., and Bunch, L. (2017) Revisiting the quinoxalinedione scaffold in the construction of new ligands for the ionotropic glutamate receptors, *ACS Chem. Neurosci. 8*, 2477-2495.

(11) Møllerud, S., Kastrup, J. S., and Pickering, D. S. (2016) A pharmacological profile of the high-affinity GluK5 kainate receptor, *Eur. J. Pharmacol. 788*, 315-320.

(12) Lubisch, W., Behl, B., and Hofmann, H. P. (1995) Novel amido quinoxaline diones, their production and use, Google Patents.

(13) Bailey, K., and Tan, E. W. (2005) Synthesis and evaluation of bifunctional nitrocatechol inhibitors of pig liver catechol-O-methyltransferase, *Bioorg. Med. Chem. 13*, 5740-5749.

(14) Nishioka, H., Nagasawa, M., and Yoshida, K. (2000) Regioselective dealkylation of 2-alkoxybenzoic acid and its amide derivatives with aliphatic amines, *Synthesis*, 243-246.

(15) Møllerud, S., Frydenvang, K., Pickering, D. S., and Kastrup, J. S. (2017) Lessons from crystal structures of kainate receptors, *Neuropharmacology 112*, 16-28.

(16) Chen, V. B., Arendall, W. B., 3rd, Headd, J. J., Keedy, D. A., Immormino, R. M., Kapral, G. J., Murray, L. W., Richardson, J. S., and Richardson, D. C. (2010) MolProbity: all-atom structure validation for macromolecular crystallography, *Acta Crystallogr., Sect. D: Biol. Crystallogr. 66*, 12-21.

(17) Krissinel, E., and Henrick, K. (2007) Inference of macromolecular assemblies from crystalline state, *J. Mol. Biol. 372*, 774-797.

(18) Hald, H., Naur, P., Pickering, D. S., Sprogøe, D., Madsen, U., Timmermann, D. B., Ahring, P. K., Liljefors, T., Schousboe, A., Egebjerg, J., Gajhede, M., and Kastrup, J. S. (2007) Partial agonism and antagonism of the ionotropic glutamate receptor iGLuR5: structures of the ligand-binding core in complex with domoic acid and 2-amino-3-[5-tert-butyl-3-(phosphonomethoxy)-4-isoxazolyl]propionic acid, *J. Biol. Chem. 282*, 25726-25736.

(19) Pøhlsgaard, J., Frydenvang, K., Madsen, U., and Kastrup, J. S. (2011) Lessons from more than 80 structures of the GluA2 ligand-binding domain in complex with agonists, antagonists and allosteric modulators, *Neuropharmacology 60*, 135-150.

(20) Dürr, K. L., Chen, L., Stein, R. A., De Zorzi, R., Folea, I. M., Walz, T., McHaourab, H. S., and Gouaux, E. (2014) Structure and dynamics of AMPA receptor GluA2 in resting, pre-open, and desensitized states, *Cell 158*, 778-792.

(21) Alushin, G. M., Jane, D., and Mayer, M. L. (2011) Binding site and ligand flexibility revealed by high resolution crystal structures of GluK1 competitive antagonists, *Neuropharmacology 60*, 126-134.

(22) Assaf, Z., Larsen, A. P., Venskutonyte, R., Han, L., Abrahamsen, B., Nielsen, B., Gajhede, M., Kastrup, J. S., Jensen, A. A., Pickering, D. S., Frydenvang, K., Gefflaut, T., and Bunch, L. (2013) Chemoenzymatic synthesis of new 2,4-syn-functionalized (S)-glutamate analogues and structure-activity relationship studies at ionotropic glutamate receptors and excitatory amino acid transporters, *J. Med. Chem. 56*, 1614-1628.

(23) Frydenvang, K., Pickering, D. S., Greenwood, J. R., Krogsgaard-Larsen, N., Brehm, L., Nielsen, B., Vogensen, S. B., Hald, H., Kastrup, J. S., Krogsgaard-Larsen, P., and Clausen, R. P. (2010) Biostructural and pharmacological studies of bicyclic analogues of the 3-isoxazolol glutamate receptor agonist ibotenic acid, *J. Med. Chem. 53*, 8354-8361.

(24) Møllerud, S., Pinto, A., Marconi, L., Frydenvang, K., Thorsen, T. S., Laulumaa, S., Venskutonyte, R., Winther, S., Moral, A. M. C., Tamborini, L., Conti, P., Pickering, D. S., and Kastrup, J. S. (2017) Structure and affinity of two bicyclic glutamate analogues at AMPA and kainate receptors, *ACS Chem. Neurosci. 8*, 2056-2064.

(25) Alcaide, A., Marconi, L., Marek, A., Haym, I., Nielsen, B., Møllerud, S., Jensen, M., Conti, P., Pickering, D. S., and Bunch, L. (2016) Synthesis and pharmacological characterization of the selective GluK1 radioligand (*S*)-2-amino-3-(6[^{3}H]-2,4-dioxo-3,4-dihydrothieno[3,2-*d*]pyrimidin-1(*2H*)-yl)propanoic acid ([^{3}H]-NF608), *MedChemComm 7*, 2136-2144.

(26) Weston, M. C., Schuck, P., Ghosal, A., Rosenmund, C., and Mayer, M. L. (2006) Conformational restriction blocks glutamate receptor desensitization, *Nat. Struct. Mol. Biol. 13*, 1120-1127.

(27) Venskutonyte, R., Butini, S., Coccone, S. S., Gemma, S., Brindisi, M., Kumar, V., Guarino, E., Maramai, S., Valenti, S., Amir, A., Valades, E. A., Frydenvang, K., Kastrup, J. S., Novellino, E., Campiani, G., and Pickering, D. S. (2011) Selective kainate receptor (GluK1) ligands structurally based upon 1*H*-cyclopentapyrimidin-2,4(1*H*,3*H*)-dione: synthesis, molecular modeling, and pharmacological and biostructural characterization, *J. Med. Chem. 54*, 4793-4805.

(28) Naur, P., Vestergaard, B., Skov, L. K., Egebjerg, J., Gajhede, M., and Kastrup, J. S. (2005) Crystal structure of the kainate receptor GluR5 ligand-binding core in complex with (S)-glutamate, *FEBS Lett. 579*, 1154-1160.

(29) Kabsch, W. (2010) Xds, *Acta Crystallogr., Sect. D: Biol. Crystallogr. 66*, 125-132.

(30) Winn, M. D., Ballard, C. C., Cowtan, K. D., Dodson, E. J., Emsley, P., Evans, P. R., Keegan, R. M., Krissinel, E. B., Leslie, A. G., McCoy, A., McNicholas, S. J., Murshudov, G. N., Pannu, N. S., Potterton, E. A., Powell, H. R., Read, R. J.,

Vagin, A., and Wilson, K. S. (2011) Overview of the CCP4 suite and current developments, *Acta Crystallogr., Sect. D: Biol. Crystallogr. 67*, 235-242.

(31) McCoy, A. J., Grosse-Kunstleve, R. W., Adams, P. D., Winn, M. D., Storoni, L. C., and Read, R. J. (2007) Phaser crystallographic software, *J. Appl. Crystallogr. 40*, 658-674.

(32) Adams, P. D., Afonine, P. V., Bunkoczi, G., Chen, V. B., Davis, I. W., Echols, N., Headd, J. J., Hung, L. W., Kapral, G. J., Grosse-Kunstleve, R. W., McCoy, A. J., Moriarty, N. W., Oeffner, R., Read, R. J., Richardson, D. C., Richardson, J. S., Terwilliger, T. C., and Zwart, P. H. (2010) PHENIX: a comprehensive Python-based system for macromolecular structure solution, *Acta Crystallogr., Sect. D: Biol. Crystallogr. 66*, 213-221.

(33) Moriarty, N. W., Grosse-Kunstleve, R. W., and Adams, P. D. (2009) electronic Ligand Builder and Optimization Workbench (eLBOW): a tool for ligand coordinate and restraint generation, *Acta Crystallogr., Sect. D: Biol. Crystallogr. 65*, 1074-1080.

(34) Emsley, P., Lohkamp, B., Scott, W. G., and Cowtan, K. (2010) Features and development of Coot, *Acta Crystallogr., Sect. D: Biol. Crystallogr. 66*, 486-501.

(35) Mayer, M. L., Ghosal, A., Dolman, N. P., and Jane, D. E. (2006) Crystal structures of the kainate receptor GluR5 ligand binding core dimer with novel GluR5-selective antagonists, *J. Neurosci. 26*, 2852-2861.

(36) Hayward, S., and Berendsen, H. J. C. (1998) Systematic analysis of domain motions in proteins from conformational change: New results on citrate synthase and T4 lysozyme, *Proteins: Struct., Funct., Genet. 30*, 144-154.

Table of Contents Graphic